BOR DERGİSİ
JOURNAL OF BORON
http://dergipark.gov.tr/boron

Synthesis and characterization of Mn_2B nanocrystals by mechanical alloying method

Tuncay Şimşek[1]*, Telem Şimşek[2], Şadan Özcan[3]

[1]Mersin University, Architecture Faculty, Department of Industrial Design, Mersin, Turkey, ORCID ID orcid.org/0000-0002-4683-0152

[2]Hacettepe University, Department of Physics Engineering, 06800 Ankara, Turkey, ORCID ID orcid.org/0000-0003-4852-2230

[3]Hacettepe University, Department of Physics Engineering, Division of Nanotechnology and Nanomedicine, 06800 Ankara, Turkey Orcid ID orcid.org/0000-0001-7966-1845

ARTICLE INFO

Article history:
Received 17 August 2018
Revised form 30 October 2018
Accepted 11 January 2019
Available online 16 March 2019

Research Article

DOI: 10.30728/boron.454311

Keywords:
Mn_2B,
Nanoparticle,
Mechanical alloying,
Magnetic properties

ABSTRACT

In this study, elemental Mn and B initial materials were used to synthesize pure Mn_2B nanocrystals by ball milling. Milling experiments were conducted with high-energy planetary ball mill in a hardened steel vial with hardened steel balls, under Ar atmosphere at 40:1 ball-to-powder ratio and 300 rpm rotating speed. As synthesized Mn_2B nanocrystals phase structures and morphological/microstructural investigation were analyzed by X-Ray diffractometry (XRD) and scanning electron microscopy with energy-dispersive X-ray spectroscopy (SEM/EDX), respectively. Particle size of Mn_2B were calculated as 34.5 nm by Rietveld refinement. Furthermore, the magnetic behavior of nanocrystals were determined by vibrating sample magnetometer (VSM). Mn_2B sample shows ferromagnetic behavior at room temperature with saturation magnetization of 13 emu/g and coercivity of 90 Oe.

1. Introduction

The properties such as relatively high melting temperature, hardness and brittleness makes the transition metal boride of manganese as good candidates in the hard materials. Hard materials are used commonly as cutting tools and hard coating in various industrial fields [1]. Numerous synthesis methods have been used for the production of refractory borides such as combustion synthesis, which is also known as self-propagating high-temperature synthesis (SHS), solvothermal, carbothermal and mechanical alloying (MA) methods [2-5]. Among these methods, MA is intensively preferred for the advantages such as relatively low-cost equipment, simplicity, low-temperature processing, great flexibility in the selection of the processing parameters, and ability to produce large quantities of material with the same physical properties [6-9]. The powders are subjected to continuous cold-welding, flattened, fracturing and re-welding mechanisms due to impacts on the balls and grinding medium. A lot of unique alloying materials such as nanocrystalline, quasicrystalline, amorphous and supersaturated solid solutions alloys can be synthesized with this method [6]. In the literature, it is obvious that metal borides studies with MA method have exponentially increased in recent years due to its simple and favorable features [10-12].

The boron and its alloys form various compounds and alloys with many elements found in nature. In the literature, there are many allotropic phases of boron with transition elements. [13-16]. Five different solid state phases have been reported in the Mn-B binary phase diagram: the phase of Mn_2B (tetragonal structure of the Al_2Cu type, I4/mcm), MnB (orthorhombic structure of Fe-B type, Pnma), Mn_3B_4 (orthorhombic structure of the Ta_3B_4 type, Immm), MnB_2 (hexagonal structure of the AlB_2 type, P6/mmm), and MnB_4 (monoclinic structure of the MnB_4, C2/m). [1, 17-21]. However, there is a lack of available information on the synthesis of manganese borides in the literature. Meng et al. synthesized various kinds of manganese borides by liquid-solid reaction from manganese and amorphous boron powders at high pressure and high temperature. They have reported that mixing the boron and manganese powder at various atomic ratios, temperatures and pressures, Mn_4B, Mn_2B, MnB, Mn_3B_4, MnB_2, MnB_4, and MnB_x phases were synthesized effectively [22]. In another study conducted by Zhu et al., MnB alloy was synthesized by starting from Mn and B chips with arc melter [23]. Guo et al. conducted high-pressure synthesis experiments of single-crystal of MnB_2 and characterized their structure and hardness. They also theoretically examined the relative stability, as well as mechanical, electronic, and magnetic properties of MnB_2 in both the AlB_2- and ReB_2-type structures by means of first-principles calculations within DFT [24]. There are also studies by an arc melting methods for synthesis of Mn_xB_{100-x} and $Mn_xB_{45}Co_{100-x}$ alloys [25-26]. In this study, to the best of our knowledge, Mn_2B was

*Corresponding author: tuncaysimsek@mersin.edu.tr

synthesized for the first time with Mn and B powders mixture by using planetary type ball under Ar atmosphere. The phase and morphological structures were investigated with X-Ray Powder Diffractometry and crystal structures were analyzed by Rietveld refinement and scanning electron microscopy with energy-dispersive X-ray spectroscopy (SEM/EDX). Magnetic properties of as-synthesized sample was characterized by using vibrating sample magnetometer (VSM).

2. Materials and methods

The Mn_2B was synthesized by mechanical milling. Mn (Alfa Aesar, 99%) and B (Alfa Aesar, crystalline 98%,) were used as initial materials. Sample preparation and milling experiments were conducted under Argon gas (99.5%) atmosphere. Milling experiments were performed using high-energy planetary ball mill (Retch, PM 100 CM, Monomill) with hardened steel balls and hardened steel vial. Milling experiments were performed at 300 rpm rotating speed and 40:1 ball to powder ratio and prolonged up to 10 h. The purification of the obtained powders was not required. Milling conditions were given in Table 1. The reaction for preparation of Mn_2B powder is given in Eq 1. Appropriate amounts (Eq.1) of initial powders were weighted in glove box using precision balance.

$$2\,Mn + B \longrightarrow Mn_2B \qquad (1)$$

Rigaku D-max B horizontal diffractometer with CuKα radiation at a scanning rate of 0.02−1s.

Table 1. Milling conditions

Milling conditions	
Vial material	Hardened steel
Ball material	Hardened steel
Ball diameter (mm)	15
Ball to powder ratio	40:1
Rotation speed (rpm)	300
Milling period (h)	0-10 h

Phase and structural analysis of as-made nanocrystals were analyzed via X-Ray Diffractometry (Rigaku, D/MAX B horizontal diffractometer) using Cu-Kα radiation at 40 kV and 30 mA, anode voltage and current for 2θ range from 20° to 100° at a scanning rate of 0.02−1s. International Center for Diffraction Data (ICDD) powder diffraction files were used in the identification of crystalline phases. The crystal structure of the synthesized Mn_2B phase was studied by multiphase Rietveld method using MAUD software [27]. Crystallography Open Database is used for the .cif files in the refinement. For the refinement of peak profiles, the Pseudo-Voigt function is used. Morphological and microstructural characterizations were determined by scanning electron microscopy with energy-dispersive X-ray spectroscopy (SEM/EDX) using a FEI-Quanta FEG 450 microscope operated at 12.3 kV in secondary electron mode. The magnetic behavior of particles were determined using vibrating sample magnetometer (VSM) module of Physical Properties Measurement System (PPMS, Quantum Design).

3. Results and discussion

The Mn-B binary phase diagram is given in Figure 1. As seen in Figure 1, Mn_2B phase has tetragonal structure of the Al_2Cu type (space group; I4/mcm) while other phases such as MnB has orthorhombic structure of Fe-B type (space group; Pnma), Mn_3B_4 has orthorhombic structure of the Ta_3B_4 type (space group; Immm), MnB_2 has hexagonal structure of the AlB_2 type, (space group; P6/mmm), and MnB_4 has monoclinic structure of the MnB_4 (space group; C2/m) [1]. The Al_2Cu-type Mn_2B phase is easy to produce with low calculated enthalpy of formation as shown in Figure 1.

The phase analyses and microstructures of the initial materials mixtures are given in Figure 2 and Figure 3. As seen from the Figure 2, the reflections related to crystalline Mn (ICDD Card No:32-0637, Cubic, I-43m)

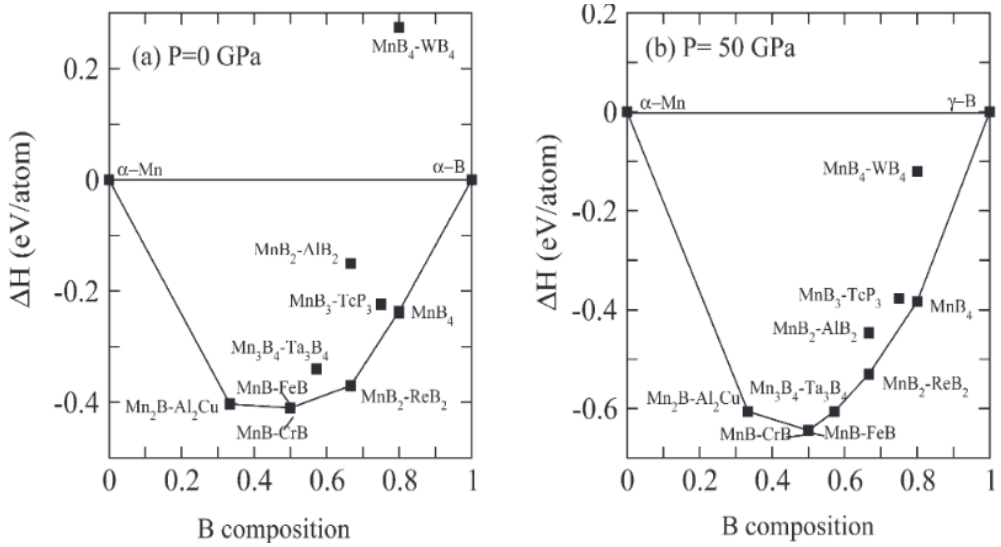

Figure 1. MnB phase diagram at a pressure of 0 and 50 GPa [1].

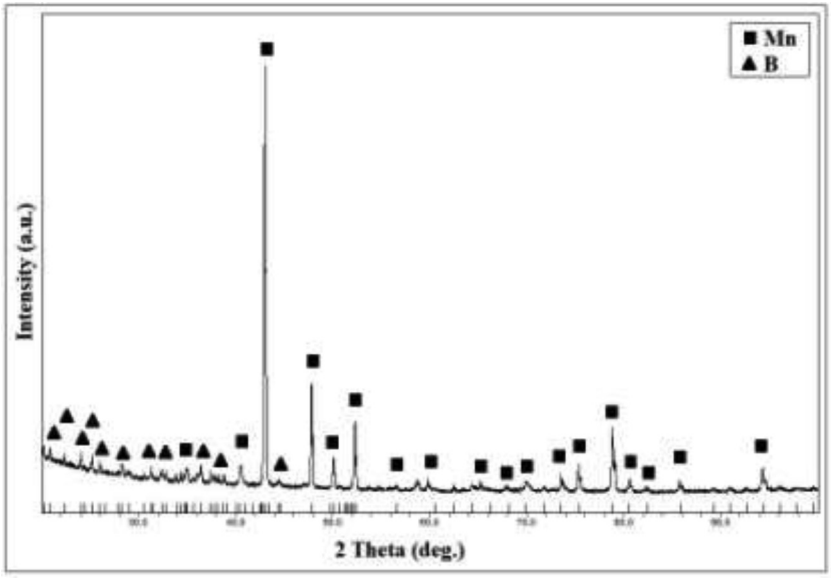

Figure 2. XRD pattern of the initial materials.

and B (ICDD Card No:31-0207, Hexagonal, R-3m) were observed in diffraction pattern. The SEM images of initial powders reveal that both of Mn and B powders were in irregular shape and morphology and size range of the B powder before milling was in the 2-200 μm while Mn was in the range of 450 nm-5 μm.

The mixed powders were ball milled for 10 hours (Table 1) and weight ratio of milling balls to powder charge ratio is 40:1. XRD pattern of the sample ball milled are given in Figure 4. The XRD pattern shows that Mn_2B phase was successfully occurred after 10 h of ball milling processes. Multiphase Rietveld refinement showed that all the Mn_2B reflections are observed (ICDD Card No: 00-025-0535) and sample is single phase. Refinements confirm the tetragonal structure of Mn_2B in I4/mcm space group with the lattice parameters of a=b=5.142 (1) Å and c=4.165 (2) Å. The structural parameters obtained from Rietveld refinements are summarized in Table 2. After progressive cold-welding, flattened and fracturing mechanisms, reactions takes place at low temperature and particle size reduce to 34.5 nm.

Figure 5 shows the SEM image of the synthesized Mn_2B nanocrystals. It is seen that size of Mn_2B particles are within the range of 50-500 nm, and have irregular/coaxial shape and morphologies. It has been also

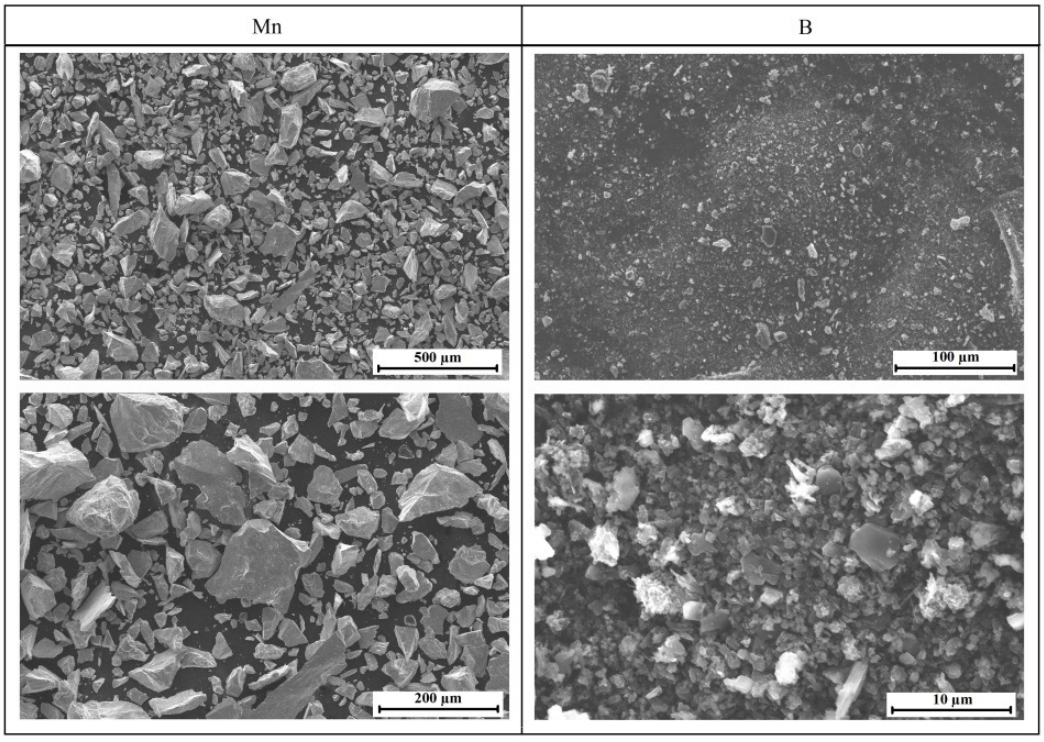

Figure 3. SEM images of the initial materials.

Table 2. Phase structures of Mn_2B nanocrystals.

Crystal system- Space group	a (Å)	b (Å)	c (Å)	Particle size
Tetragonal- I4/mcm	5.142(1)	=a	4.165(2)	34.5 ± 0.9
2θ (degree)	**hkl**	**I_f Relative intensity %**	**$d_{calculation}$ Å**	**$d_{experimental}$ Å**
24.435	110	10.0	3.6400	3.6494
34.826	200	15.0	2.5740	2.6050
42.952	002	25.0	2.1040	2.0952
44.833	211	100.0	2.0200	2.0185
50.020	112	11.0	1.8220	1.8180
56.441	202	25.0	1.6290	1.6228
73.461	312	12.0	1.2880	1.2861
78.767	330	9.0	1.2140	1.2170
80.029	213	30.0	1.1980	1.2006
84.017	420	1.0	1.1510	1.1460
89.102	402	6.0	1.0980	1.0923

observed that particles are agglomerated. It is known that particle size reduction takes due to some mechanisms such as cold welding, flattening and repeated fractures in mechanical alloying processing. Consequently, new unstable surfaces are formed by continuous fractures and deformations, and as a result agglomeration occurs. The EDX elemental analysis confirms the Mn and B phases together with little Cr and Fe impurities. Due to the nature of the milling process, impurities are frequently observed originating from to the milling vial.

In order to obtain information about the magnetic properties, magnetic field dependence of magnetization (M(H)) of the as-made Mn_2B powder is measured at 300 K (Figure 6). This measurement can be divided into 4 quadrants. In the 1st quadrant, external magnetic field is applied to powder sample and swept from 0 – 3 T range, which is also called virgin curve. Magnetization of the sample was measured continuously under the applied field. Then in the second quadrant, magnetic field is swept from 3 – 0 T. The direction of the applied field was then reversed during the 3rd quadrant and field is applied from 0 – (-3) T. Finally applied field was swept from -3 – 0 T in the 4rd quadrant and magnetization of the sample was measured continuously. Significant physical parameters such as; saturation magnetization, saturation field, coercivity, anisotropy constant and maximum energy product can be obtained from M(H) measurement. As can be seen in Figure 4, Mn_2B sample has weak ferromagnetic signal with the saturation magnetization of 13 emu/g. Sample has coercivity of 90 Oe at 300 K, as depicted in the inset of figure. Among the manganese borides only MnB with positive exchange interaction between Mn atoms shows ferromagnetic behavior while MnB_2 and Mn_3B_4 are antiferromagnetic. MnB_4 phase is paramagnetic and Mn_2B is non-magnetic [28]. The ferromagnetic behavior observed in our sample (Figure 6) could be attributed to the small amount of Fe/Cr impurities, which originates from milling experiment carried using hardened steel vial.

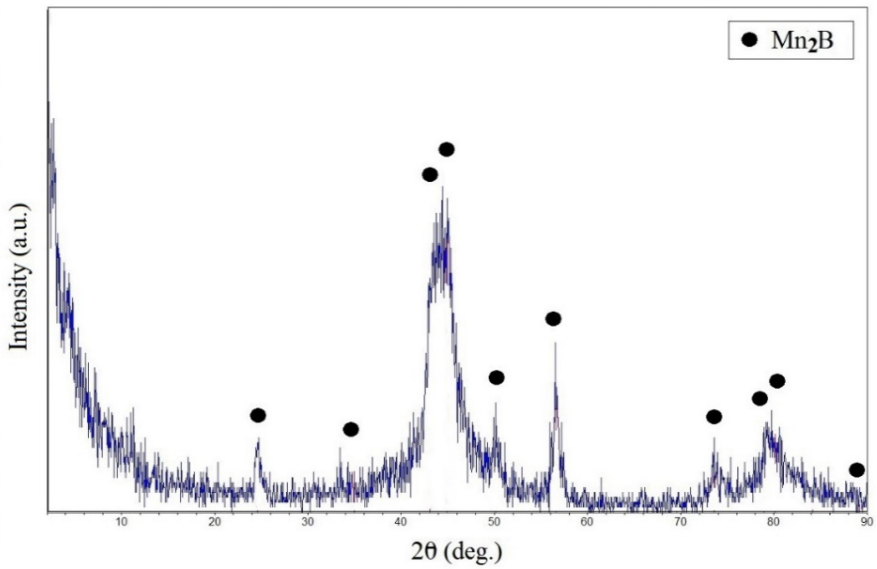

Figure 4. XRD patterns of 10h milled Mn_2B nanocrystals before and after leaching. Indexing the Mn_2B hase is done using tetragonal unit cell (ICDD Card No: 00-025-0535).

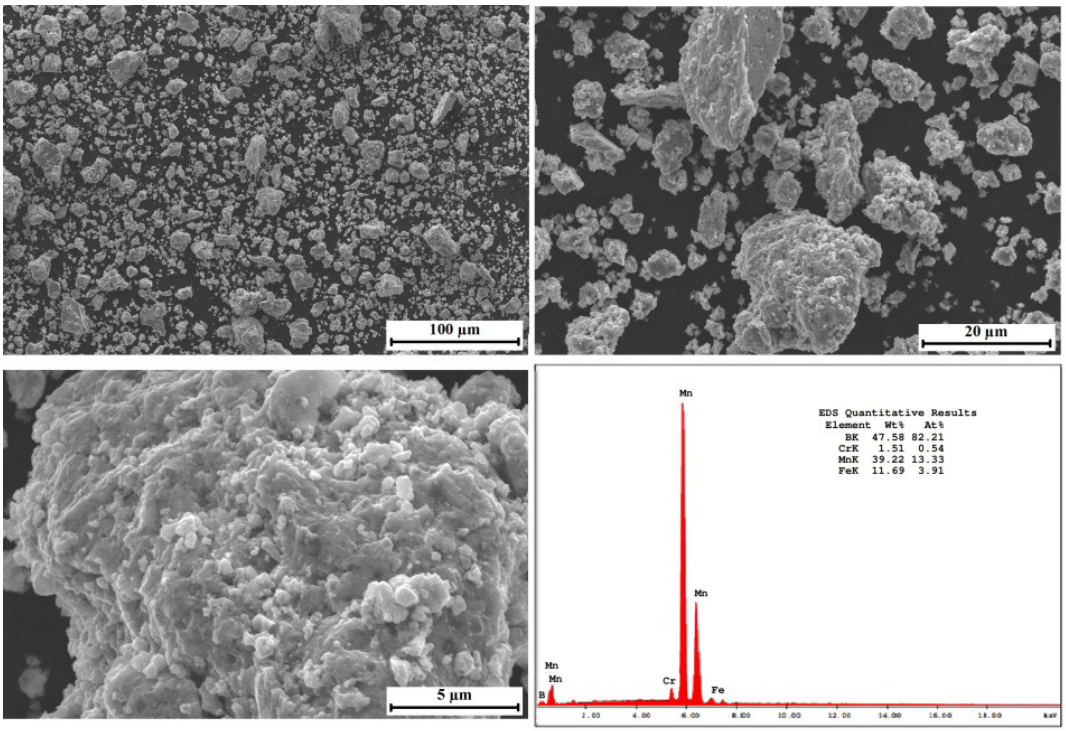

Figure 5. SEM images and EDX elemental analysis of the as-synthesized Mn_2B powders.

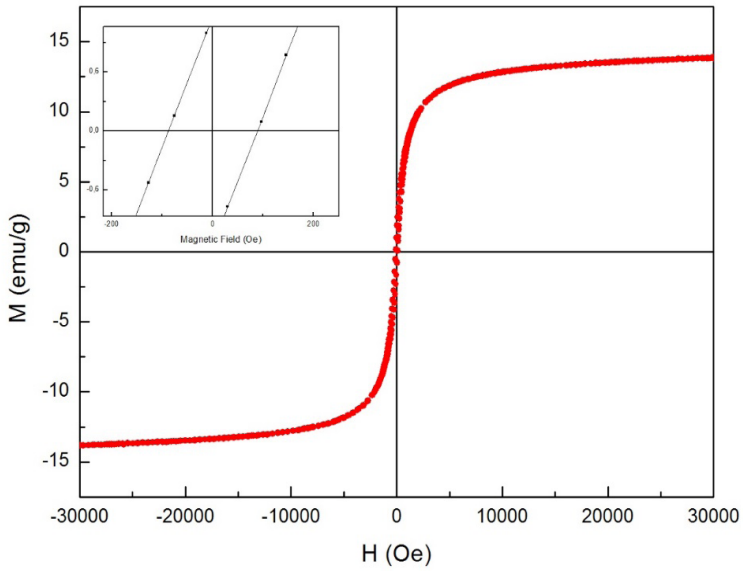

Figure 6. Room temperature M(H) curve of the synthesized Mn_2B.

4. Conclusion

The synthesis of Mn_2B nanocrystals were studied with the initial powders of Mn and B at 300 rpm rotating speed and 40:1 ball to powder ratio via planetary ball mill. It is seen that after 10 h ball milling Mn_2B nanocrystals were synthesized. The synthesized particles are characterized using x-ray diffraction/spectroscopy, electron microscopy, and vibrating sample magnetometer measurements. Particle sizes of the nanocrystals were calculated as 34.5 nm by Rietveld refinement. In contrary to the reported works in the literature, Mn_2B sample was found to be ferromagnetic at room temperature with small saturation magnetization of 13 emu/g. This weak ferromagnetic signal is attributed to the Fe impurity caused from the hardened steel milling vial.

References

[1] Wang B., Li X., Wang Y.X., Tu Y.F., Phase Stability and physical properties of manganese borides: A first-principles study, J. Phys. Chem. C, 115, 21429–21435, 2011.

[2] Liu G., Li J., Chen K., Combustion synthesis of refractory and hard materials: A review, Int. J. Refract. Met. Hard Mater., 39, 90–102, 2013.

[3] Kang S. H., Kim D. J., Synthesis of nano-titanium di-

boride powders by carbothermal reduction, J. Eur. Ceram. Soc., 27, 715–718, 2007.

[4] Barış M., Şimşek T., Taşkaya H., Chattopadhyay A.K., Synthesis of Fe-Fe_2B catalysis via solvothermal route for hydrogen generation by hydrolysis of $NaBH_4$, BORON, 3 (1) 51-62, 2018.

[5] Y., Zhang J., Zou C., Lin H.T., An L., Zhang F., Wang C., Synthesis of osmium borides by mechanochemical method, J. Am. Chem. Soc., 100 (6), 2419-2428, 2017.

[6] Suryanarayana C., Mechanical Alloying and Milling, 1st edition, Marcel Dekker, New York, 2004.

[7] Avar B., Ozcan S., Characterization and amorphous phase formation of mechanically alloyed $Co_{60}Fe_5Ni_5Ti_{25}B_5$ powders, J. Alloys Compd., 650, 53-58, 2015.

[8] Suryanarayana C., Phase formation under non-equilibrium processing conditions: rapid solidification processing and mechanical alloying, J. Mater. Sci., 53 (19), 13364–13379, 2018.

[9] Avar B., Simsek T., Gogebakan M., Mekanik alaşımlama ile üretilen Nanokristal $Fe_{60}Al_{30}Cu_{10}$ (at.%) tozların yapısal ve mekanik özellikleri, G.U. J. Sci. Part C, 7 (1) 184-191, 2019.

[10] Simsek, T, Baris M, Kalkan B, Mechanochemical processing and microstructural characterization of pure Fe2B nanocrystals, Adv. Powder Technol., 28 (11), 3056-3062, 2017.

[11] Adil S., Karati A., Murty B.S., Mechanochemical synthesis of nanocrystalline aluminium boride (AlB12), Ceram. Int., 44 (16), 20105-20110, 2018.

[12] Long Y., Zhang J., Zou C., Lin H.T., An L., Zhang F., Wang C., Synthesis of osmium borides by mechanochemical method, J. Am. Ceram. Soc., 100, 2419–2428, 2017.

[13] Bilen B., Gürü M., Çakanyildirim Ç., Conversion of KCl into KBH4 by Mechano-Chemical Reaction and its Catalytic Decomposition, Journal of Electronic Materials, 46 (7), 4126–4132, 2017.

[14] Kalay S., Yilmaz Z., Sen O., Emanet M., Kazanc E., Çulha M., Synthesis of boron nitride nanotubes and their applications, Beilstein J. Nanotechnol., 6, 4–102, 2015.

[15] Mohammad O. T., Golabgir H., Tajizadegan H., Jamshidi A., Mechanochemical behavior of magnesium–boron oxide–melamine ternary system in the synthesis of h-BN nanopowder, Ceram. Int., 42 (5) 6450-6456, 2016.

[16] Makarenko G. N., Krushinskaya L. A., Timofeeva I. I., Matsera V. E., Vasil'kovskaya M. A., Uvarova I. V., Formation of diborides of groups iv–vi transition metals during mechanochemical synthesis, Powder Metall. Met. Ceram., 53, 514–521, 2015.

[17] Kadomatsu H., Ishii F., Fujiwara H., Magnetization, Lattice Constants and Hydrostatic Pressure Effect on the Curie Temperature of (Co1−xMnx)2B, J. Phys. Soc. Jpn., 47, 1078–1085, 1979.

[18] Wong-Ng W., Mc Murdie H. F., Paretzkin B., Zhang Y., Davis K. L., Hubbard C. R., Dragoo A. L., Stewart J. M., Standard X-ray diffraction powder patterns of sixteen ceramic phases, Powder Diffr., 2, 191–201, 1987.

[19] Cely A., Tergenius L. E., Lundstrom T. J., Microhardness measurements and phase analytical studies in the MnB system, Powder Diffr., 61, 193–198, 1978.

[20] Ishii T., Shimada M., Koizumi M.J., Exchange striction of ferromagnetic solid solution of (Mn1-xTax)3B4, Journal of Applied Physics, 54, 6907, 1983.

[21] Andersson S., Carlsson J. O., Crystal Structure of MnB4, Acta Chemica Scandinavica, 24, 1791–1799, 1970.

[22] Meng X., Bao K., Zhu P., He Z., Tao Q., Li J., Mao Z., Cui T., Manganese borides synthesized at high pressure and high temperature, J. Appl. Phys., 111, 112616, 2012.

[23] Zhu H., Ni C., Zhang F., Du Y., Xiao J. Q., Fabrication and magnetic property of MnB alloy, J. Appl. Phys., 97, 10M512, 2005.

[24] Gou H., Steinle G., Bykova E., Nakajima Y., Miyajima N., Li Y., Ovsyannikov S. V., Dubrovinsky L.S., Dubrovinskai N., Stability of MnB2 with AlB2-type structure revealed by first-principles calculations and experiments, Appl. Phys. Lett., (102), 061906, 2013.

[25] Piyan C., Simsek T., Kaynar B., Özcan S., Fabrication and Magnetic Properties of MnxB45Co100−x Alloys, J. Supercond. Novel Magn., 29 (8), 2203–2206, 2016.

[26] Simsek T., Ozcan S., Structural and Magnetic Properties of MnxB100-x Alloys, IEEE Trans. Magn., 51, 1-1, 2015.

[27] L. Lutterotti, MAUD CSD Newslett, IUCr, 24, 2000.

[28] Ma S., Bao K., , Tao Q., Zhu P., Ma T., Liu B., Liu Y., Cui T., Manganese mono-boride, an inexpensive room temperature ferromagnetic hard material, Scientific Reports, 7, 1-9, 2017.